Research Article | Vol. 29, No. 9 / 26 April 2021 / Optics Express 14025
Optics EXPRESS

Planar refractive lenses made of SiC for high intensity nanofocusing

MIKHAIL LYUBOMIRSKIY,[1,*] BART SCHURINK,[2] IGOR A. MAKHOTKIN,[2] DENNIS BRUECKNER,[1,3,4] FELIX WITTWER,[1,4] MAIK KAHNT,[5] MARTIN SEYRICH,[1,4] FRANK SEIBOTH,[1] FRED BIJKERK,[2] AND CHRISTIAN G. SCHROER[1,4]

[1]*Deutsches Elektronen-Synchrotron DESY, Notkestraße 85, 22607 Hamburg, Germany*
[2]*Industrial Focus Group XUV Optics, MESA+ Institute for Nanotechnology, University of Twente, Drienerlolaan 5, 7522 NB Enschede, The Netherlands*
[3]*Ruhr-University Bochum, Faculty of Chemistry and Biochemistry, Universitätsstr. 150, 44801 Bochum, Germany*
[4]*Department Physik Universität Hamburg, Luruper Chaussee 149, 22761 Hamburg, Germany*
[5]*MAX IV Laboratory, Lund University, 22100 Lund, Sweden*
[*]*mikhail.lyubomirskiy@desy.de*

Abstract: We report on the manufacturing and testing of the first nanofocusing refractive lenses made of single-crystal silicon carbide. We introduce the fabrication process based on lithography, followed by deep isotropic etching. The lenses were characterized at the energy of 12 keV at the beamline P06 of the synchrotron radiation source PETRA III. A focal spot of 186 nm×275 nm has been achieved with a lens working distance of 29 mm.

1. Introduction

The rapid development of new-generation light sources such as ultralow-emittance synchrotron radiation sources and X-ray free-electron lasers (XFELs) [1–4] opens up new opportunities in many fields of science, from physics, chemistry, biology, and medicine to geo- and materials science, and nanotechnology. Their increased spectral brightness up to the high-energy X-ray range enables efficient focusing to locally probe complex materials down to the nanoscale, probing physical and chemical properties quantitatively using various X-ray analytical techniques. In turn, this requires X-ray optics with minimal aberrations to focus the X-rays to the diffraction limit and preserve the coherence. Due to the short wavelengths, the requirements on the shape and materials properties of X-ray optics are extreme.

In the regime of hard X-rays, refractive lenses are very attractive due to many outstanding properties [5]. To date, the most commonly used type of refractive lenses are rotationally parabolic lenses [6,7]. They are used at many beamlines for focusing and beam conditioning [5]. Due to limitation in the manufacturing process, it is currently not possible to make lenses with radii of curvature of much smaller than 50 µm, which results in a comparably long focal lengths. As the numerical aperture of refractive lenses increases with decreasing focal length, the diffraction-limited spot size generated by these optics is limited. This limit can be overcome by so-called nanofocusing refractive lenses made by lithographic fabrication schemes, i. e., resulting in a more compact design allowing for much shorter focal lengths [8]. The reduced focal length results in a larger numerical aperture and thus a smaller diffraction-limited focal spot.

So far, the material for nanofocusing lenses was mainly limited to silicon [8,9], thanks to well-developed manufacturing and structuring approaches. Modern technologies for micro-electro-mechanical systems (MEMS) allow micro-structuring of Si crystals with the high quality

#416223 https://doi.org/10.1364/OE.416223
Journal © 2021 Received 30 Dec 2020; revised 31 Mar 2021; accepted 12 Apr 2021; published 23 Apr 2021

Optics EXPRESS

needed for X-ray optics. To-date, the highest spatial resolution achieved with Si refractive planar optics is around 20 nm [10]. Nevertheless, Si is not an ideal material for X-ray optics, as the relatively strong attenuation limits the numerical aperture and transmission of the optics, thus limiting the spatial resolution and flux in X-ray microscopy experiments. In addition, Si is not well suited for high-power load applications, due to poor heat conductivity ($\sim 140\,\mathrm{W\,m^{-1}\,K^{-1}}$ at room temperature) and low melting point (1685 °K) [11].

On the other hand, diamond is a well-suited material for the manufacturing of high-power load lenses. It has large thermal conductivity of around $2000\,\mathrm{W\,m^{-1}\,K^{-1}}$ at room temperature. Consequently refractive lenses made from diamond have an improved thermal load management [12]. Diamond lenses also have better transmission for X-rays and a higher numerical aperture due to the lower absorption compared with higher-Z materials. However, the manufacturing of diamond lenses is very challenging, as diamond is chemically and physically very stable. Therefore, progress has been slow in the development of diamond-based refractive X-ray optics: since the fabrication of the very first diamond lens more than 15 years ago [13], little progress has been made and neither molded [14] nor structured [15] diamond lenses can reach the optical performance of those made of Si.

Despite the great need for high-resolution refractive optics that can handle high flux, SiC has not been considered so far as lens material. Being a semiconductor material, it has many outstanding properties: it has a very high thermal conductivity (up to $500\,\mathrm{W\,m^{-1}\,K^{-1}}$ at room temperature), low thermal expansion, and a high melting point (3100 K) that provides high thermal stability [16]. In addition, nano-fabrication techniques for SiC are well established and provide a solid basis for the production of high-quality X-ray optics. The patterning of SiC wafer requires high energetic species to dissociate the present strong inter-atomic silicon-carbon bonds in the anisotropic SiC material. The most obvious method for the etching of SiC is by high plasma densities and ion energies, as achieved by dry etchers [17–19]. As a result of this, SiC can be etched in a way comparable to the fabrication of Si nanofocusing lenses [8]. In this article, we present the very first lenses made of SiC. While the fabrication parameters for this first set of optics were not fully optimized in particular in view of the aperture, the fabrication process is scalable and will allow to make lenses with optimized (numerical) aperture. In the following, we describe the fabrication process and show first X-ray optical results.

2. SiC optical properties

To prove the advantages of SiC for the X-ray optics application, let us compare its focusing performance with Si, as it is the most common material to manufacture lenses for nanofocusing. Due to the presence of atoms of carbon and more dense packing, SiC has 40 % higher density in comparison with Si. This leads to larger refractive power, Fig. 1 shows real and imaginary parts of the refractive index for Si and SiC in the energy range of $8 - 30$ keV. It is easy to see that SiC has about 40 % larger δ and very similar β. As a result, it is allowing to achieve the same focusing length with fewer lenses, which leads to a decrease of the diffraction limit.

For instance, to achieve the focal distance of 7 mm with 20 keV irradiation, it requires 130 Si lenses with a radius of 2 µm and only 92 SiC lenses with the same radius. Besides, to achieve two-dimensional focusing, the second array of lenses needs to be arranged in crossed geometry, which increases the total number of lenses in the beam and results in a significant difference in a total lens transmission. The total lens transmission difference between Si and SiC then is a factor of four. Besides, for SiC, smaller total lens absorption leads to enlarged effective aperture and reduced diffraction limit, increasing the gain. Finally, SiC lens has a reduced amount of absorbed heat that the lens needs to dissipate during the operation as there is less material needed to refract the beam for similar NA.

Optics EXPRESS

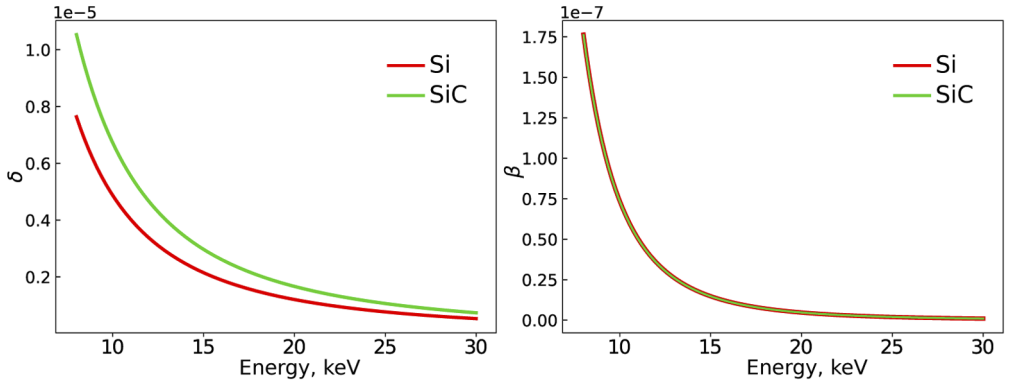

Fig. 1. Real (left) and imaginary (right) parts of the complex refractive index of Si and SiC for the energy range of 8 − 30 keV.

3. Lens fabrication

For lens manufacturing, a 4 inch n-type 4H-SiC (0001) substrate (Norstel) was used. The substrate was covered with a metal mask consisting of a sputtered 20 nm Chromium adhesion layer and atop a 350 nm Nickel layer as a hard mask. On top of Ni, a 1.7 µm photoresist layer was deposited using spin-coating. As a masking material, Nickel is selected based on its high theoretical selectivity over SiC compared to other potential contenders as SiN, SiO_2, and Photoresist [20]. By means of conventional lithography, a spin-coated layer of photoresist was exposed (EVG 620 aligner) with UV using a chromium-based lithography mask (roughly 10 % loading). After the development of the photoresist, the exposed metal mask was ion beam etched (Oxford i300 RIBE) utilizing the SIMS endpoint detection to stop the etch at the SiC interface. The photoresist was removed by acetone and isopropanol. The dry etching of SiC was performed using settings based on available literature [21,22] and our existing knowledge on the etching of Silicon.

An inductively coupled plasma reactive ion etcher (ICP-RIE) system with fluorine chemistry was utilized for etching of SiC. Here, fluorine in the form of SF_6 was chosen as it tends to produce more volatile products compared to, for instance, chlorine etch chemistry. In addition to SF_6, O_2 was used to further the formation of the volatile species utilized to mask the sidewall and promote anisotropic etching.

The substrate was etched in 10 min intervals using an Adixen AMS 100DE ICP-RIE (Alcatel). The following settings were used: source to substrate distance is 120 mm, process pressure of 0.02 mbar, temperature of 20 °C (Helium backside cooling) and ICP of 2500 W, RF power of 225 W, 200 sccm of SF_6 and 20 sccm of O_2. The etch depth was inspected by the stylus surface profilometer (Bruker Dektak 150), and the geometry was inspected by HR-SEM (FEI Sirion) after removal of the Ni mask by a mixture of nitric acid, Acetic acid, Sulfuric acid in DI water (5:5:1:5).

The 4H-SiC substrate is etched for a total of 30 min at which the Ni mask was starting to be removed from the center outwards. At this stage, an etch depth of 18 µm was achieved, which translates to an etch rate of 0.6 µm min^{-1} and a Ni mask selectivity of 51 over the SiC. A sidewall angle of 92° was measured by SEM observation (not shown). The etch produced a bottom surface with a relatively low roughness without the formation of micropillars (Fig. 2), which indicates the absence of surface defects and redeposition of masking material during the etch [23,24]. Furthermore, the first couple of micrometers of the sidewall have very low roughness with some slight tapering. At this stage, during the etch, the sidewall is not yet covered by volatile reaction products and is thus etching underneath the mask without the addition of surface roughness. After these initial etched micrometers, the sidewall tapering is reduced at the

Optics EXPRESS

expense of introduced roughness, mediated by the continuous deposition and partial etching of volatile reaction products (Fig. 2). The observed sidewall roughness is similar to that presented in literature [20,22–24] and can potentially be prevented by optimizing the etch recipe to prevent excessive deposition of reaction products. In addition, such optimization is also expected to lead to a further increase in the etch rate and mask selectivity.

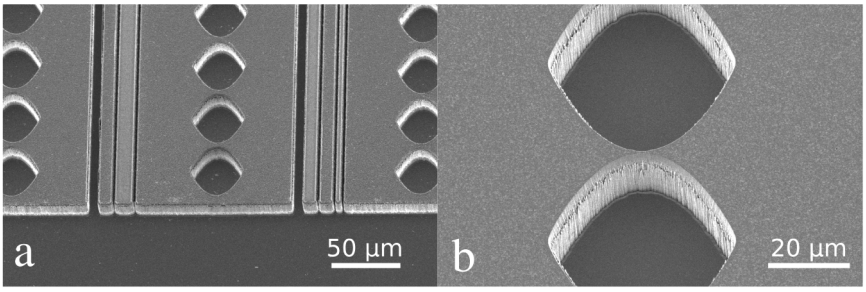

Fig. 2. (a) SEM observation of multiple lens arrays etched in the 4H-SiC substrate by SF_6/O_2 in a ICP-RIE system after removal of the Nickel mask. (b) Close-up of two lenses, indicating a smooth bottom surface and a side wall roughness associated with masking effects during etching.

4. Focusing performance results

The focusing capabilities of the produced SiC lenses were studied at the P06 beamline of PETRA III. The beam profile generated by these lenses was studied using ptychography [25]. In this method, an object is scanned through a coherent beam, while a far-field diffraction pattern is recorded at each scan position. Both the object's complex transmission function and the probing complex wave-field are reconstructed from the diffraction patterns and the knowledge of their relative positions in the scan. As a result, even if the object is not in the exact focus position, it is still possible to propagate the reconstructed probing wave-field determined at the sample position numerically to the focal plane and characterize the focal spot. Ptychography has proven to be a standard technique for the characterization of optics [26–31].

The experimental scheme is depicted in Fig. 3. A desired harmonic with an energy of 12.0 keV was selected by a channel-cut Si-(111) monochromator. Undesired higher harmonics were cut-off by a pair of total reflection mirrors. Lenses were positioned in the beam using a pair of SmarAct piezo hexapods providing full geometrical freedom. Downstream from the lenses, a two-dimensional resolution test chart (Siemens Star) manufactured by NTT-AT was situated close to the expected focus position at a lens working distance of $f = 29$ mm downstream from the last lens chip, and after the first reconstruction was shifted to the beam's smallest waist, a final ptychographic scan was performed again. The Eiger 4M detector [32] was placed at 3420 mm distance from the sample position. The optical path between source and lens position was around 98 m. Because the lenses had limited depth due to small thickness of the etching mask, a combination with the smallest geometric aperture was chosen: a horizontally focusing lens comprised of 29 bi-concave lenses with the radius of 7.06 µm in combination with a vertically focusing lens comprised of 16 bi-concave lenses with the radius of 7.26 µm. The distance between individual lenses in parabola apex was 2 µm. The full geometric aperture (limited by the etching depth) of the combined optics was around 18 µm in both directions. The expected theoretical focus size for this lens stack is $d = 125$ nm in horizontal direction and is $d = 200$ nm in vertical, the total lens transmission is $T = 0.26$. The estimation for the lens focus size and total transmission has been performed based on the well-known formalism [7] taking into account the source of a size of $\sigma = 60$ µm in horizontal direction and is $\sigma = 22$ µm in vertical.

Optics EXPRESS

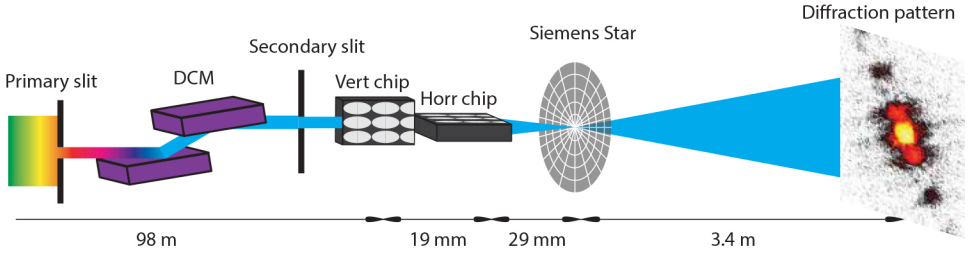

Fig. 3. Schematic of the ptychography setup of the P06 beamline at PETRA III.

Figures 4(a) and 4(b) show the beam profiles in horizontal and vertical planes generated by numerical propagation through the focus of the wave-field reconstructed via ptychography. Figures 4(c) and 4(d) show corresponding cross-sections through focal plane. The size of the focal spot (FWHM) is $d = (186 + /-2)$ nm in horizontal and is $d = (275 + /-3)$ nm in vertical directions respectively, which is about 40 % larger than expected.

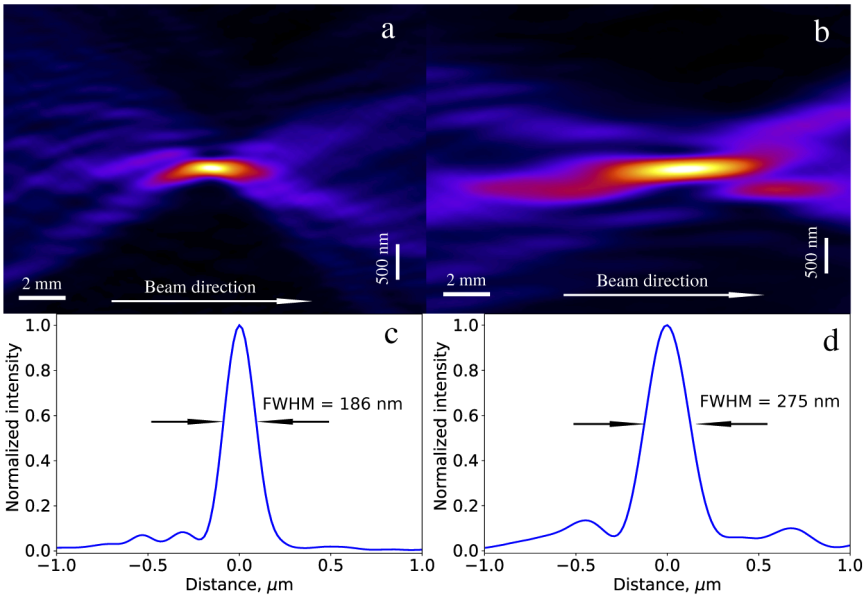

Fig. 4. Beam profiles, in horizontal – (a) and vertical – (b) directions, generated by numerical propagation of the reconstructed wave fields. Corresponding cross sections in horizontal – (c) and vertical – (d) directions, respectively.

Moreover, a slight beam splitting downstream of the focus indicates the presence of spherical aberrations due to deviation of the lens shape from perfect parabola; this can be eliminated by introducing mask correction for the over-etching effect.

To assess the lens arrangement's deviations from the perfect parabolic shape, the wave-field was numerically propagated to the horizontal lens exit plane, and a spherical component was subtracted. The resulting complex wave-field is depicted in Fig. 5. It is easy to see that the lens focusing performance was limited by two factors: lens etching depth and deviations from perfect parabolic shape. The aperture of the horizontal lens was not illuminated entirely, which is indicated by the absence of intensity on the right side of the complex wave-field in the Fig. 5. The

Optics EXPRESS

change of the color across the wave-field along both vertical and horizontal directions indicates spherical aberrations.

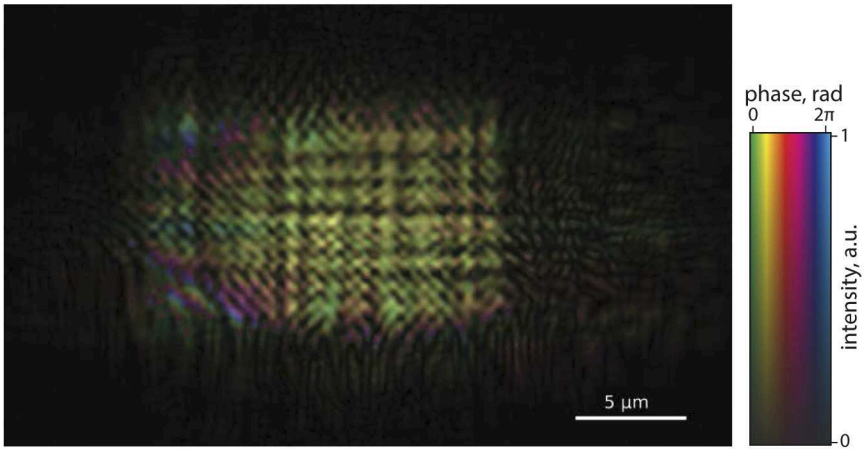

Fig. 5. A complex wave-field at the horizontal lens exit plane. A spherical component is subtracted. The phase is color-coded.

5. Conclusions

In this first experiment, X-ray lenses were etched in a 4H-SiC substrate by ICP RIE with SF_6/O_2 chemistry. We obtained lenses etched with sidewalls with 92° angle and a smooth etched bottom surface. The maximal etch depth with the given etch recipe and nickel mask was 18 µm, thus a mask selectivity of 51 was achieved. During optimization of the etching parameters, the mask thickness turned out to be a primary limiting factor for the etching depth. The use of a mask with larger thickness is not associated with technical challenges. It will increase the etching depth and, as a result, the geometric aperture of the lens can be fully illuminated in the future. The lenses demonstrated good focusing performance, nevertheless not perfect. The measured focus size was about 40 % larger than the theoretical optimum for the design lens geometry, which can be explained by the influence of a limited etching depth, surface roughness, and deviation from parabolic shape. In order to eliminate these effects, the etching process has to be optimized, and mask correction has to be introduced. Moreover, we plan to use the mask with greater thickness for future trials to achieve a larger etching depth.

Funding. Deutsche Forschungsgemeinschaft ((DFG)–SFB 1441–Project-ID 426888090); Netherlands Organization of Research FRAME project (ref nr 15357).

Acknowledgments. We acknowledge DESY (Hamburg, Germany), a member of the Helmholtz Association HGF, for the provision of experimental facilities. Parts of this research were carried out at PETRA III and we would like to thank Gerald Falkenberg and Jan Garrevoet for assistance in using P06 beamline. M.S. was partly funded by the Deutsche Forschungsgemeinschaft (DFG)–SFB 1441–Project-ID 426888090. D. B. acknowledges core funding of the Helmholtz Imaging Platform (HIP), a platform of the Helmholtz Incubator on Information and Data Science. We additionally acknowledge the FRAME project (ref nr 15357) carried out at the XUV group at the University of Twente, and funded by the Netherlands Organization of Research.

Disclosures. The authors declare no conflicts of interest.

References

1. P. F. Tavares, S. C. Leemann, M. Sjöström, and Å. Andersson, "The MAXIV storage ring project," J. Synchrotron Radiat. **21**(5), 862–877 (2014).
2. P. F. Tavares, E. Al-Dmour, A. Andersson, F. Cullinan, B. N. Jensen, D. Olsson, D. K. Olsson, M. Sjöström, H. Tarawneh, S. Thorin, and Å. Vorozhtsov, "Commissioning and first-year operational results of the MAXIV 3GeV ring," J. Synchrotron Radiat. **25**(5), 1291–1316 (2018).

Optics EXPRESS

3. C. Bostedt, S. Boutet, D. M. Fritz, Z. Huang, H. J. Lee, H. T. Lemke, A. Robert, W. F. Schlotter, J. J. Turner, and G. J. Williams, "Linac coherent light source: The first five years," Rev. Mod. Phys. **88**(1), 015007 (2016).
4. C. G. Schroer, I. Agapov, W. Brefeld, R. Brinkmann, Y.-C. Chae, H.-C. Chao, M. Eriksson, J. Keil, X. Nuel Gavaldà, R. Röhlsberger, O. H. Seeck, M. Sprung, M. Tischer, R. Wanzenberg, and E. Weckert, "Petra iv: the ultralow-emittance source project at desy," J. Synchrotron Radiat. **25**(5), 1277–1290 (2018).
5. M. Lyubomirskiy and C. G. Schroer, "Refractive Lenses for Microscopy and Nanoanalysis," Synchrotron Radiat. News **29**(4), 21–26 (2016).
6. C. G. Schroer, M. Kuhlmann, B. Lengeler, T. F. Gunzler, O. Kurapova, B. Benner, C. Rau, A. S. Simionovici, A. A. Snigirev, and I. Snigireva, "Beryllium parabolic refractive x-ray lenses," in *Design and Microfabrication of Novel X-Ray Optics*, vol. 4783 D. C. Mancini, ed., International Society for Optics and Photonics (SPIE, 2002), pp. 10–18.
7. B. Lengeler, C. Schroer, J. Tümmler, B. Benner, M. Richwin, A. Snigirev, I. Snigireva, and M. Drakopoulos, "Imaging by parabolic refractive lenses in the hard X-ray range," J. Synchrotron Radiat. **6**(6), 1153–1167 (1999).
8. C. G. Schroer, M. Kuhlmann, U. T. Hunger, T. F. Günzler, O. Kurapova, S. Feste, F. Frehse, B. Lengeler, M. Drakopoulos, A. Somogyi, A. S. Simionovici, A. Snigirev, I. Snigireva, C. Schug, and W. H. Schräder, "Nanofocusing parabolic refractive x-ray lenses," Appl. Phys. Lett. **82**(9), 1485–1487 (2003).
9. C. G. Schroer, O. Kurapova, J. Patommel, P. Boye, J. Feldkamp, B. Lengeler, M. Burghammer, C. Riekel, L. Vincze, A. van der Hart, and M. Küchler, "Hard x-ray nanoprobe based on refractive x-ray lenses," Appl. Phys. Lett. **87**(12), 124103 (2005).
10. J. Patommel, S. Klare, R. Hoppe, S. Ritter, D. Samberg, F. Wittwer, A. Jahn, K. Richter, C. Wenzel, J. W. Bartha, M. Scholz, F. Seiboth, U. Boesenberg, G. Falkenberg, and C. G. Schroer, "Focusing hard x rays beyond the critical angle of total reflection by adiabatically focusing lenses," Appl. Phys. Lett. **110**(10), 101103 (2017).
11. C. J. Glassbrenner and G. A. Slack, "Thermal Conductivity of Silicon and Germanium from 3 °K to the Melting Point," Phys. Rev. **134**(4A), A1058–A1069 (1964).
12. J. E. Field, *The Properties of diamond* (Academic, 1979).
13. A. Snigirev, V. Yunkin, I. Snigireva, M. Di Michiel, M. Drakopoulos, S. Kouznetsov, L. Shabel'nikov, M. Grigoriev, V. Ralchenko, I. Sychov, M. Hoffmann, and E. Voges, "Diamond refractive lens for hard X-ray focusing," Proc. SPIE **4783**, 1–9 (2002).
14. O. J. L. Fox, L. Alianelli, A. M. Malik, I. Pape, P. W. May, and K. J. S. Sawhney, "Nanofocusing optics for synchrotron radiation made from polycrystalline diamond," Opt. Express **22**(7), 7657–7668 (2014).
15. M. Lyubomirskiy, P. Boye, J. M. Feldkamp, J. Patommel, S. Schoeder, A. Schropp, M. Burghammer, C. Wild, and C. G. Schroer, "Diamond nanofocusing refractive X-ray lenses made by planar etching technology," J. Synchrotron Radiat. **26**(5), 1554–1557 (2019).
16. M. E. Levinshtein, S. L. Rumyantsev, and M. Shur, *Properties of advanced semiconductor materials : GaN, AlN, InN, BN, SiC, SiGe* (Wiley, 2001).
17. K. Xie, J. R. Flemish, J. H. Zhao, W. R. Buchwald, and L. Casas, "Low damage and residue–free dry etching of 6h–sic using electron cyclotron resonance plasma," Appl. Phys. Lett. **67**(3), 368–370 (1995).
18. J. Wang, E. Lambers, S. Pearton, M. Ostling, C.-M. Zetterling, J. Grow, F. Ren, and R. Shul, "Icp etching of sic," *Solid State Electron.* pp. 2283–2288 (1998).
19. G. McDaniel, J. W. Lee, E. S. Lambers, S. J. Pearton, P. H. Holloway, F. Ren, J. M. Grow, M. Bhaskaran, and R. G. Wilson, "Comparison of dry etch chemistries for sic," J. Vac. Sci. Technol., A **15**(3), 885–889 (1997).
20. K. M. Dowling, A. J. Suria, A. Shankar, C. A. Chapin, and D. G. Senesky, "Multilayer etch masks for 3-dimensional fabrication of robust silicon carbide microstructures," in *2015 28th IEEE International Conference on Micro Electro Mechanical Systems (MEMS)*, (2015), pp. 284–287.
21. F. A. Khan and I. Adesida, "High rate etching of sic using inductively coupled plasma reactive ion etching in sf6-based gas mixtures," Appl. Phys. Lett. **75**(15), 2268–2270 (1999).
22. P. Chabert, "Deep etching of silicon carbide for micromachining applications: Etch rates and etch mechanisms," J. Vac. Sci. Technol., B **19**(4), 1339–1345 (2001).
23. N. Okamoto, "Elimination of pillar associated with micropipe of SiC in high-rate inductively coupled plasma etching," J. Vac. Sci. Technol., A **27**(2), 295–300 (2009).
24. L. F. Voss, K. Ip, S. J. Pearton, R. J. Shul, M. E. Overberg, A. G. Baca, C. Sanchez, J. Stevens, M. Martinez, M. G. Armendariz, and G. A. Wouters, "SiC via fabrication for wide-band-gap high electron mobility transistor/microwave monolithic integrated circuit devices," J. Vac. Sci. Technol., B **26**(2), 487–494 (2008).
25. F. Pfeiffer, "X-ray ptychography," Nat. Photonics **12**(1), 9–17 (2018).
26. A. Schropp, P. Boye, J. M. Feldkamp, R. Hoppe, J. Patommel, D. Samberg, S. Stephan, K. Giewekemeyer, R. N. Wilke, T. Salditt, J. Gulden, A. P. Mancuso, I. A. Vartanyants, E. Weckert, S. Schöder, M. Burghammer, and C. G. Schroer, "Hard x-ray nanobeam characterization by coherent diffraction microscopy," Appl. Phys. Lett. **96**(9), 091102 (2010).
27. C. M. Kewish, P. Thibault, M. Dierolf, O. Bunk, A. Menzel, J. Vila-Comamala, K. Jefimovs, and F. Pfeiffer, "Ptychographic characterization of the wavefield in the focus of reflective hard x-ray optics," Ultramicroscopy **110**(4), 325–329 (2010).
28. J. Vila-Comamala, A. Diaz, M. Guizar-Sicairos, A. Mantion, C. M. Kewish, A. Menzel, O. Bunk, and C. David, "Characterization of high-resolution diffractive x-ray optics by ptychographic coherent diffractive imaging," Opt. Express **19**(22), 21333–21344 (2011).

Optics EXPRESS

29. A. Schropp, R. Hoppe, J. Patommel, D. Samberg, F. Seiboth, S. Stephan, G. Wellenreuther, G. Falkenberg, and C. G. Schroer, "Hard x-ray scanning microscopy with coherent radiation: Beyond the resolution of conventional x-ray microscopes," Appl. Phys. Lett. **100**(25), 253112 (2012).
30. A. Kubec, S. Braun, S. Niese, P. Krüger, J. Patommel, M. Hecker, A. Leson, and C. G. Schroer, "Ptychography with mulitlayer Laue lenses," J. Synchrotron Radiat. **21**(5), 1122–1127 (2014).
31. M. Lyubomirskiy, F. Koch, K. A. Abrashitova, V. O. Bessonov, N. Kokareva, A. Petrov, F. Seiboth, F. Wittwer, M. Kahnt, M. Seyrich, A. A. Fedyanin, C. David, and C. G. Schroer, "Ptychographic characterisation of polymer compound refractive lenses manufactured by additive technology," Opt. Express **27**(6), 8639 (2019).
32. I. Johnson, A. Bergamaschi, H. Billich, S. Cartier, R. Dinapoli, D. Greiffenberg, M. Guizar-Sicairos, B. Henrich, J. Jungmann, D. Mezza, A. Mozzanica, B. Schmitt, X. Shi, and G. Tinti, "Eiger: A single-photon counting x-ray detector," J. Instrum. **9**(05), C05032 (2014).